Bismuth chalcohalides and oxyhalides as optoelectronic materials

Hongliang Shi,[1,2] Wenmei Ming,[1] and Mao-Hua Du[1]
[1]*Materials Science and Technology Division and Center for Radiation Detection Materials and Systems, Oak Ridge National Laboratory, Oak Ridge, Tennessee 37831, USA*
[2]*Key Laboratory of Micro-Nano Measurement, Manipulation, and Physics (Ministry of Education), School of Physics and Nuclear Energy Engineering, Beihang University, Beijing 100191, China*
(Received 7 August 2015; revised manuscript received 11 March 2016; published 29 March 2016)

Several Tl and Pb based halides and chalcohalides have recently been discovered as promising optoelectronic materials [i.e., photovoltaic (PV) and gamma-ray detection materials]. Efficient carrier transport in these materials is attributed partly to the special chemistry of ns^2 ions (e.g., Tl^+, Pb^{2+}, and Bi^{3+}). However, the toxicity of Tl and Pb is challenging to the development and the wide use of Tl and Pb based materials. In this paper, we investigate materials that contain Bi^{3+}, which is also an ns^2 ion. By combining Bi halides with Bi chalcogenides or oxides, the resulting ternary compounds exhibit a wide range of band gaps, offering opportunities in various optoelectronic applications. Density functional calculations of electronic structure, dielectric properties, optical properties, and defect properties are performed on selected Bi^{3+} based chalcohalides and oxyhalides, i.e., BiSeBr, BiSI, BiSeI, and BiOBr. We propose different applications for these Bi compounds based on calculated properties, i.e., *n*-BiSeBr, *p*-BiSI, and *p*-BiSeI as PV materials, BiSeBr and BiSI as room-temperature radiation detection materials, and BiOBr as a *p*-type transparent conducting material. BiSeBr, BiSI, and BiSeBr have chain structures while BiOBr has a layered structure. However, in BiSI, BiSeI, and BiOBr, significant valence-band dispersion is found in the directions perpendicular to the atomic chain or layer because the valence-band edge states are dominated by the halogen states that have strong interchain or interlayer coupling. We find significantly enhanced Born effective charges and anomalously large static dielectric constants of the Bi compounds, which should reduce carrier scattering and trapping and promote efficient carrier transport in these materials. The strong screening and the small anion coordination numbers in Bi chalcohalides should lead to weak potentials for electron localization at anion vacancies. Defect calculations indeed show that the anion vacancies (Se and Br vacancies) in BiSeBr are shallow, which is beneficial to efficient electron transport.

DOI: 10.1103/PhysRevB.93.104108

I. INTRODUCTION

Recently many halides that contain ns^2 ions (ions with outer electron configuration of ns^2, e.g., Tl^+, Pb^{2+}, Bi^{3+}, and Sn^{2+}) have been discovered as potentially useful optoelectronic materials. For examples, solar cells based on halide perovskites (e.g., $CH_3NH_3PbI_3$) have achieved power conversion efficiency >20% [1,2]; several Tl compounds (e.g., TlBr, Tl_6SeI_4, and Tl_6SI_4) exhibit excellent carrier transport efficiency and are being developed as room-temperature semiconductor radiation detectors [3–6]. The success of these halides as optoelectronic materials is closely related to the properties of ns^2 ions [7–11]. As schematically shown in Fig. 1, in a halide with ns^2 cations, the fully occupied cation *s* band hybridizes with the anion *p* band, resulting in a dispersive valence band. The conduction band is dominated by the spatially extended cation *p* states, which hybridize with the anion *p* states of the valence band, giving rise to significant cross-band-gap hybridization in a halide. This could lead to a mixed ionic-covalent character, which is known to enhance lattice polarization significantly [12,7,10]. Therefore, a halide with ns^2 ions often has dispersive valence and conduction bands and a large static dielectric constant. The strong screening of charged defects and impurities reduces the rates of carrier scattering and trapping. These electronic and dielectric properties are favorable for efficient carrier transport in halides with ns^2 cations.

Since many Tl^+ and Pb^{2+} based compounds exhibit excellent carrier transport properties, Bi^{3+} based compounds should also have great potential to become high-performance optoelectronic materials with the additional benefit of not containing toxic metal elements [13]; however, they have so far attracted limited attention and have not been systematically studied. BiI_3 has been investigated as a photovoltaic (PV) material [14] and a room-temperature semiconductor radiation detector material [15]. The heavy Bi ions in Bi compounds enable strong absorption of gamma rays, an important requirement for a gamma-ray detector. There have also been several investigations of Bi chalcohalides (such as BiSI) [16,17] as solar materials and Bi oxyhalides (such as BiOI) [18,19] as photocatalytic materials. Electronic structures and optical properties of some Bi chalcohalides have previously been studied using density functional calculations [20–23]. However, these calculations did not include the spin-orbit coupling (SOC), which is important for the heavy atoms such as Tl, Pb, and Bi.

In light of the outstanding transport properties observed in many halides that contain ns^2 cations, we investigate Bi chalcohalides and oxyhalides as potential optoelectronic materials. By combining Bi halides with Bi chalcogenides or oxides, the resulting ternary compounds exhibit a wide range of band gaps (e.g., 3.455 eV for BiOCl, 2.92 eV for BiOBr, 1.89 eV for BiOI, 1.89 eV for BiSCl, 1.95 eV for BiSBr, 1.56 eV for BiSI, 1.50 eV for BiSeBr, and 1.3 eV for BiSeI) [24], which offers opportunities in various applications. For example, a material with a band gap between 1.1 and 1.6 eV, between 1.5 and 2.2 eV, or larger than 3 eV may be interesting in the area of photovoltaics, room-temperature radiation detection,

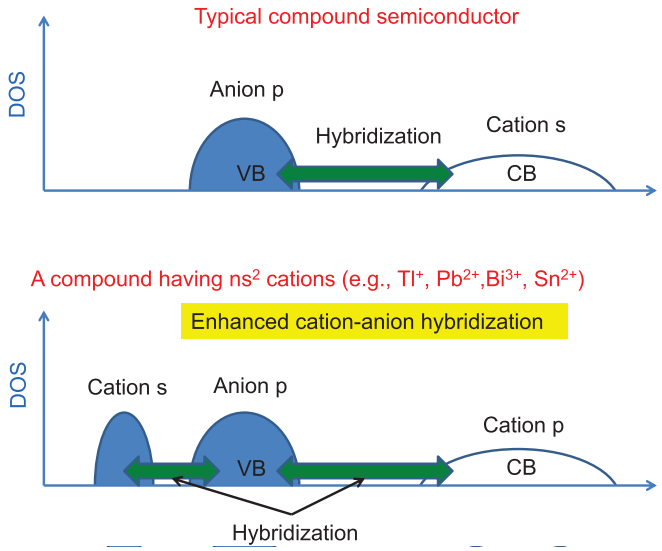

FIG. 1. Schematic of density of states for a typical compound semiconductor (not including transition-metal and rare-earth compounds with significant d or f character in the conduction band) and a compound that contains ns^2 cations.

or transparent electronics, respectively. Density functional calculations are performed to study electronic structures, dielectric properties, optical absorption, and defects in selected Bi chalcohalides and oxyhalides, i.e., BiSeBr, BiSI, BiSeI, and BiOBr. We show the potentials of BiSeBr, BiSI, and BiSeI as PV and radiation detection materials and BiOBr as a p-type transparent conducting material based on calculated material properties.

II. COMPUTATIONAL METHODS

All calculations were performed based on density functional theory. Electronic structure, Born effective charges, and dielectric constants were calculated using Perdew, Burke, and Ernzerhof (PBE) [25] functionals. Optical absorption was calculated using Tran-Blaha modified Becke-Johnson (TB-mBJ) potential functionals. The TB-mBJ functional has been shown to give good band gaps and optical properties for many semiconductors and insulators [26–28]. Charge transition levels of defects were calculated using Heyd-Scuseria-Ernzerhof (HSE) hybrid functionals [29,30], which have 25% Hartree-Fock exchange. The screening parameter of the nonlocal Fock exchange in the HSE calculations was set at 0.2 Å^{-1} (the HSE06 functional) [29]. The hybrid density functional methods have been shown to improve results on the band gap and the defect properties in semiconductors [31–35]. The charge transition level $\varepsilon(q/q')$ for a defect is determined by the Fermi level (ε_f), at which the formation energies of the defect with charge states q and q' are equal to each other. $\varepsilon(q/q')$ can be calculated using

$$\varepsilon(q/q') = \frac{E_{D,q'} - E_{D,q}}{q - q'}, \quad (1)$$

where $E_{D,q}$ ($E_{D,q'}$) is the total energy of the supercell that contains the relaxed structure of a defect at charge state q (q').

The electron-ion interactions were described using projector augmented wave potentials [36]. For calculations of electronic structure, optical, and defect properties, the valence wave functions were expanded on a plane-wave basis with a cutoff energy of 243 eV for BiSeBr, BiSeI, and BiSI, and with a higher cutoff energy of 400 eV for BiOBr. The electronic structure and the defect levels are well converged at these cutoff energies. All the cutoff energies were increased by 30% for the calculations of the Born effective charges and the dielectric constants for better accuracy on forces. PBE and HSE calculations were performed using the Vienna *ab initio* simulation package [37,38] and the TB-mBJ calculations were performed using the WIEN2K code [39]. Experimental lattice constants [24] were used for all the materials studied in this work. The SOC was used in all calculations except those of the Born charges and the ionic contribution to the static dielectric constant because, although the SOC is important for obtaining the electronic structure, it has negligible effect on the accuracy of forces.

III. RESULTS AND DISCUSSION

The band gaps of BiSeBr, BiSI, BiSeI, and BiOBr calculated using PBE, TB-mBJ, and HSE functionals are shown in Table I. The TB-mBJ and HSE band gaps are in good agreement with the experimental values (within a few percent) whereas PBE calculations underestimate the band gaps by about 30%.

BiSI, BiSeI, and BiSeBr have optical band gaps of 1.56, 1.3, and 1.5 eV [24], respectively, which are suitable for efficient solar energy absorption. These Bi chalcohalides crystallize in a structure of space group *Pnam* (No. 62). The atoms are arranged in chains along the a axis as shown in Fig. 2(a). Figures 3(a)–3(c) show the band structures of BiSI, BiSeI, and BiSeBr calculated using PBE functionals including the SOC. To understand the effect of the SOC, the band structures obtained without the SOC are shown in Fig. S1 (see the Supplemental Material [40]). Since the valence and conduction bands are both derived from p orbitals of heavy atoms, the SOC has significant effects on both the valence and the conduction bands. The conduction-band maximum (CBM) is lowered, the valence-band maximum (VBM) is raised, and the band degeneracies are lifted due to the SOC.

The band structures of the Bi chalcohalides shown in Fig. 3 all exhibit indirect band gaps. For BiSeBr, the CBM is at

TABLE I. Calculated and experimental band gaps (in eV) of BiSeBr, BiSeI, BiSI, and BiOBr. The band gaps are calculated using PBE, TB-mBJ, and HSE functionals. Spin-orbit coupling is included in all calculations. The measured direct band gaps are also shown.

	PBE		TB-mBJ		HSE	Expt. (Ref. [24])
	Indirect	Direct	Indirect	Direct	Direct	Direct
BiSeBr	0.94	1.01	1.41	1.45	1.64	1.5
BiSeI	0.89	0.94	1.31	1.40		1.3
BiSI	1.07	1.09	1.57	1.61		1.56
BiOBr	1.90	2.06	2.84	3.09		3.0

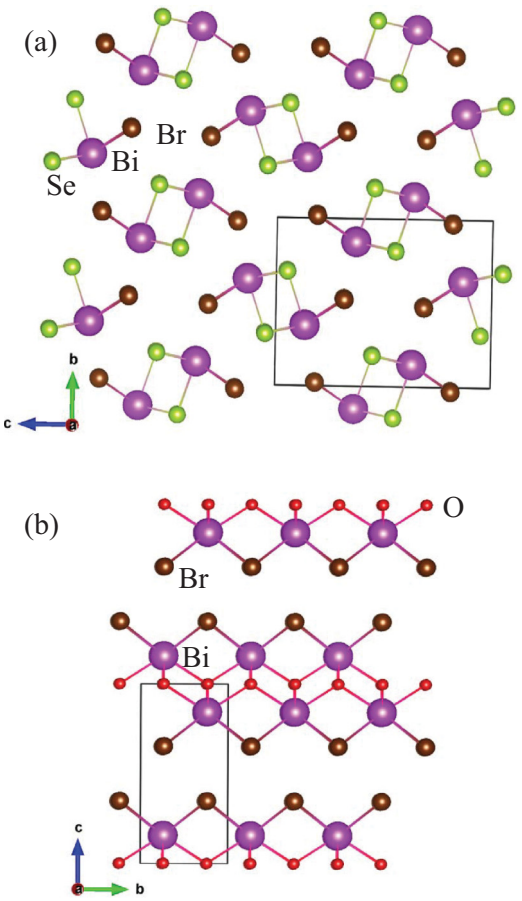

FIG. 2. Structures of (a) BiSeBr and (b) BiOBr. In (a), BiSeBr has atomic chains oriented in the a direction. Note that BiSI and BiSeI have the same crystal structure as BiSeBr.

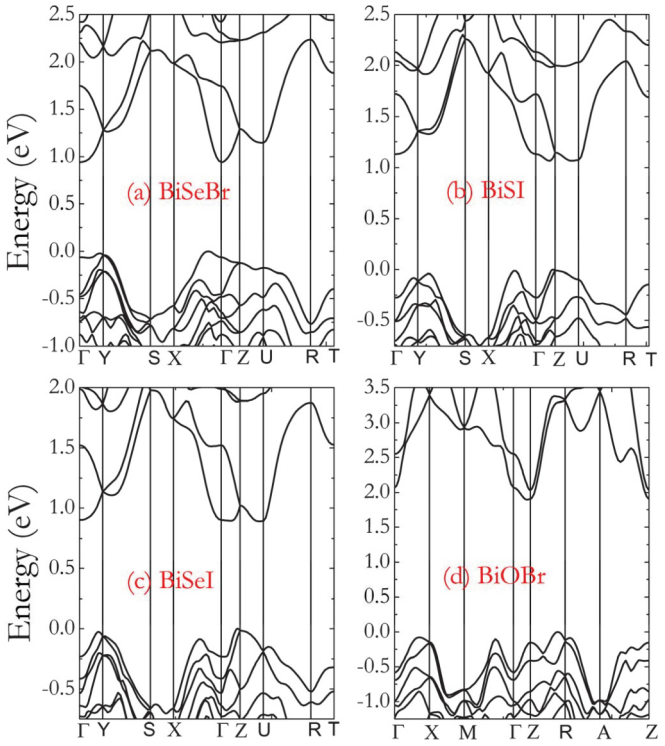

FIG. 3. Band structures of (a) BiSeBr, (b) BiSI, (c) BiSeI, and (d) BiOBr calculated using PBE functionals. The spin-orbit coupling is included. Note that the band gaps are underestimated in PBE calculations.

the Γ point while the VBM is at a k point along the Γ-X direction; the conduction and the valence bands are both most dispersive along the Γ-X direction due to the covalent bonding in the atomic chains along the a axis. For BiSI and BiSeI, the CBM and the VBM are located at k points along the Z-T and the Γ-Z directions, respectively. The conduction bands are highly nonparabolic; interestingly, the valence bands are quite dispersive in directions both parallel and perpendicular to the atomic chains.

In BiSI and BiSeI, the states near the VBM are dominated by the I $5p$ states as seen in their density of states (DOS) in Figs. 4(b) and 4(c). Despite having chain structures, the interchain I-I coupling is still strong due to the short interchain I-I distance. In BiSI, the shortest distance between the two I ions from two adjacent atomic chains is 4.01 Å, slightly shorter than the nearest-neighbor I-I distance within the atomic chain, which is 4.17 Å. Similarly, the inter- and intrachain nearest-neighbor I-I distances in BiSeI are 4.21 and 4.22 Å, respectively, which are close to each other. Furthermore, I^- is a large ion with spatially extended wave functions, thereby providing better contact and coupling between atomic chains. Therefore, the significant valence-band dispersion in BiSI and BiSeI along the directions perpendicular to the atomic chain [as seen in Figs. 3(b) and 3(c)] should be related to the significant interchain coupling between I $5p$ states, which dominate near the VBM.

In BiSeBr, the Br-Br interchain coupling should be weaker compared to the I-I interchain coupling in Bi chalco-iodides due to the more electronegative nature of Br. The electronegativities (Pauling scale) of S, Se, and I are close to each other,

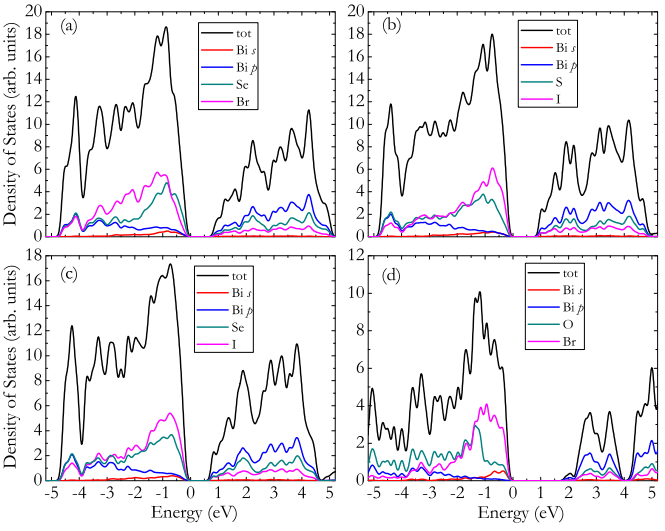

FIG. 4. Density of states for (a) BiSeBr, (b) BiSi, (c) BiSeI, and (d) BiOBr calculated using PBE functionals. The spin-orbit coupling is included. Note that the band gaps are underestimated in PBE calculations.

i.e., 2.58, 2.55, and 2.66, respectively, while that of Br is much larger, i.e., 2.96. Therefore, in BiSeBr, the states near the VBM have more Se $4p$ character than Br $4p$ character [see DOS in Fig. 4(a)]. The Se interchain coupling is relatively weak due to the large Se-Se distances. The shortest distance between Se ions from two adjacent chains (5.65 Å) is much longer than the nearest-neighbor Se-Se distance within the atomic chain (3.81 Å). Consequently, the valence-band dispersion in the directions perpendicular to the atomic chains in BiSeBr is significantly smaller than that along the chain.

The conduction bands of BiSeBr, BiSI, and BiSeI are all most dispersive along the Γ-X direction [see Figs. 3(a)–3(c)]. However, the CBMs of BiSI and BiSeI are not located at the Γ point in contrast to BiSeBr; therefore, the CBM states of BiSI and BiSeI are less dispersive than that of BiSeBr.

The DOS of BiSeBr, BiSI, and BiSeI [Figs. 4(a)–4(c)] shows significant Bi 6s character near the VBM as a result of hybridization between the Bi 6s band, which is deeply below the valence band (not shown), and the anion-p-dominated valence band, in agreement with Fig. 1. Such hybridization should increase the valence-band dispersion in Bi^{3+} based compounds as seen in other halides with ns^2 cations (e.g., TlBr and $CH_3NH_3PbI_3$) [7,10]. Chalcohalides have strong ionicity. On the other hand, there is also significant cross-band-gap hybridization between the Bi $6p$ and the anion p states as indicated by the overlap of the partial DOS of the Bi $6p$ and the anion p states in both the conduction and the valence bands [Figs. 4(a)–4(c)]. Such hybridization suggests significant covalency. The mixed ionic-covalent character is known to give rise to strong lattice polarization [7–11]. Indeed, our calculations show that the Born effective charges along the a direction (the atomic chain direction) of BiSeBr, BiSI, and BiSeI are significantly enhanced and those along the c direction (where the interchain halogen contact is significant) are also increased from their nominal ionic charges (see Table II). (The Born effective charge is a measure of how lattice polarization develops with atomic displacement.) The strong lattice polarization in Bi chalcohalides leads to anomalously large static dielectric constants (ε_{st}) along the a and c directions, in particular the a direction (see Table II);

TABLE II. Born effective charges for Bi, high-frequency dielectric constant (ε_∞), and static dielectric constant (ε_{st}) along the a, b, c directions for BiSeBr, BiSI, BiSeI, and BiOBr calculated using PBE functionals. Note that the nominal ionic charge of Bi is +3. Spin-orbit coupling is not included.

	Z^* (Bi)	ε_∞	ε_{st}
BiSeBr	5.57 (a)	10.83 (a)	57.24 (a)
	2.80 (b)	7.85 (b)	14.31 (b)
	3.84 (c)	9.18 (c)	25.10 (c)
BiSI	6.42 (a)	12.39 (a)	71.32 (a)
	3.04 (b)	8.37 (b)	14.26 (b)
	4.01 (c)	9.90 (c)	24.17 (c)
BiSeI	6.11 (a)	13.13 (a)	62.82 (a)
	2.80 (b)	9.26 (b)	14.78 (b)
	3.88 (c)	10.70 (c)	24.76 (c)
BiOBr	5.62 (a,b)	7.37 (a,b)	51.09 (a,b)
	3.43 (c)	5.49 (c)	10.26 (c)

the electronic contribution (ε_∞) is small and is likely still overestimated due to the underestimated PBE band gaps. The large static dielectric constants of Bi chalcohalides should provide strong screening of charged defects and impurities, thereby reducing carrier scattering and trapping. The efficient carrier transport in TlBr and $CH_3NH_3PbI_3$ has been attributed partly to their large static dielectric constants [7,10].

The hole effective masses of BiSI and BiSeI in the Γ-Z direction are calculated to be $0.32\,m_e$ and $0.29\,m_e$, respectively, which are small, comparable to the calculated hole effective mass of $CH_3NH_3PbI_3$ [10]. BiSI has previously been investigated as a PV material [16,17]. n-type BiSI was coupled with p-type CuSCN in a planar heterojunction thin-film solar cell [17]. The small conduction-band dispersion of BiSI and BiSeI suggests that the electron transport in BiSI and BiSeI may be inefficient. On the other hand, the hole transport should be more efficient due to the small hole effective masses. Thus, it may be of interest to investigate a solar cell with p-BiSI or p-BiSeI (as the light absorber and the hole transport material) coupled with an n-type electron transport material. A distributed heterojunction device architecture may be desirable because it allows fast electron transfer from p-BiSI or p-BiSeI to the n-type electron transport material, minimizing the impact of slow electron transport in BiSI and BiSeI.

The electron effective masses of BiSeBr are calculated to be $0.41\,m_e$ in the Γ-X direction, which is reasonably small, and $0.91\,m_e$ in the Γ-Z direction. The calculated hole effective mass of BiSeBr is $0.94\,m_e$ in the Γ-X direction. The optical band gap of 1.5 eV and reasonably good electron and hole effective masses makes BiSeBr a potential solar absorber material. The anisotropic electronic structure of BiSeBr does not necessarily prevent it from being used in a polycrystalline thin-film solar cell. Previous experimental and theoretical work showed that Sb_2Se_3, a material with a similar one-dimensional chain structure, is a promising thin-film PV material [41]. In fact, atomic chain structures may lead to intrinsically benign grain boundaries, a favorable property for polycrystalline thin-film materials [40].

BiSI, BiSeI, and BiSeBr have strong optical absorption near their respective band-gap energies, which is important for a solar absorber material. The optical absorption coefficients of BiSI, BiSeI, and BiSeBr are calculated using TB-mBJ functionals [see Figs. 5(a)–5(c)]. The onset of strong absorption ($>10^4\,cm^{-1}$) occurs at the energies very close to the direct band-gap energies. The strong optical absorption may be related to (1) the significant Bi 6s character near the VBM, which enables on-site transition between the Bi 6s and 6p states; (2) the significant cross-band-gap hybridization, which enables charge-transfer absorption; and (3) the p-orbital-derived conduction band, which has higher DOS than the typical s-orbital-derived conduction band in sp semiconductors.

A semiconductor radiation detector relies on the collection of radiation-generated free electrons and holes [42]. Since the electron and hole mobilities are usually significantly different in a compound semiconductor, a detector is often configured to collect only one type of the charge carriers. As shown above, the valence band of BiSI is much more dispersive than its conduction band and BiSI has a band gap larger than 1.5 eV. These properties suggest that BiSI is a potential

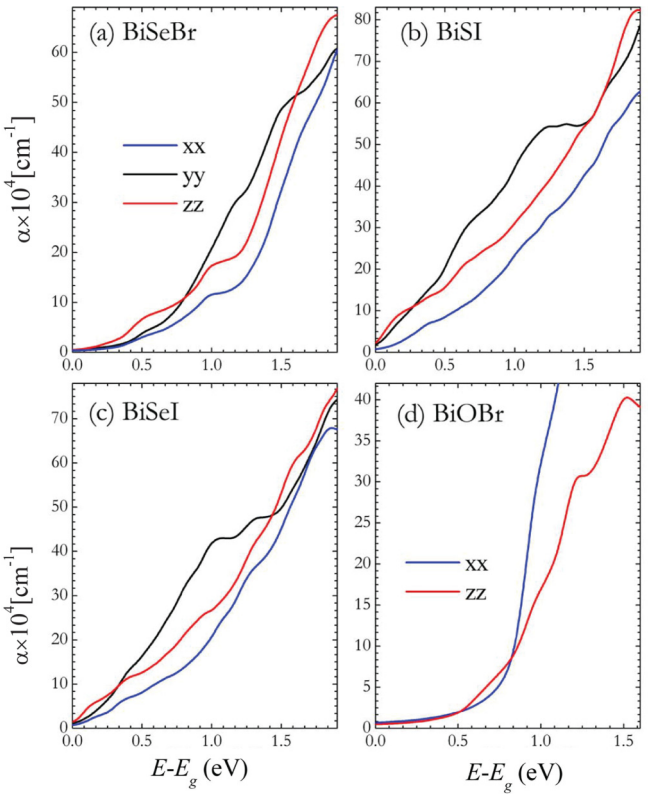

FIG. 5. Optical absorption coefficients for (a) BiSeBr, (b) BiSI, (c) BiSeI, and (d) BiOBr calculated using TB-mBJ functionals. The spin-orbit coupling is included.

room-temperature gamma-ray detection material based on hole collection. On the other hand, BiSeBr may be used as a room-temperature gamma-ray detection material based on electron collection. For a single-crystal gamma-ray detector material, it is possible to apply the electric field along a specific crystallographic direction. (Note that single crystals are required in semiconductor radiation detectors.) In the case of Bi chalcohalides, it would be preferable to apply the electric field along the direction of the atomic chains [see Fig. 2(a)]. Both BiSI and BiSeBr have large atomic masses, which make them attractive as gamma-ray detector materials because heavy atoms can efficiently absorb gamma rays. High resistivity is required for semiconductor radiation detection materials. Resistivity depends sensitively on the defect and impurity properties, which will be the subject of future studies.

Combining a Bi halide with a Bi oxide rather than a Bi chalcogenide significantly increases the band gap of the ternary Bi compound. For example, the direct band gap of BiOBr is 3 eV [24]. The mixing of the O $2p$ states and the Br $4p$ states in BiOBr results in more delocalized valence-band states than those of a pure oxide, making BiOBr a potentially interesting p-type transparent conducting material. BiOBr has a layered structure (space group $P4/nmmZ$ No. 129) as shown in Fig. 1(b). The band structure and the DOS of BiOBr calculated using PBE with the SOC are shown in Figs. 3(d) and 4(d), respectively. The states near the VBM have a strong Br $4p$ character as can be seen in Fig. 4(d). The valence bands are dispersive both on the ab plane and along the c axis. The interlayer Br coupling is significant. The shortest Br-Br interlayer distance is 3.72 Å, even shorter than the nearest-neighbor Br-Br distance on the ab plane (3.92 Å). The VBM is located along the Z-R direction. The calculated hole effective mass along the Z-R direction is $0.57\,m_e$, which compares favorably to those of other proposed p-type transparent conducting materials (such as transition metal oxides, wide-gap chalcogenides, etc.) [43,44]. The optical absorption coefficient of BiOBr [Fig. 5(d)] rises slowly above the optical band gap, which is desirable for obtaining good transparency. The Born effective charges of BiOBr are significantly enhanced on the ab plane as shown in Table II. The calculated large static dielectric constant of BiOBr should reduce the carrier scattering and trapping and enhance the hole mobility.

Defects play an important role in carrier compensation and carrier transport in optoelectronic materials. A comprehensive study of defects in all the materials discussed in this paper is beyond the scope of this work. Here, we focus on Se and Br vacancies in BiSeBr as examples to illustrate some important defect properties of anion vacancies that may be general to Bi chalcohalides. Understanding the electron trapping properties of the anion vacancies is extremely important because the anion vacancies are usually the most important electron traps in compound semiconductors. The efficient carrier transport in halide perovskite solar cells has been attributed partly to the shallow nature of the halogen vacancy [45,10,46,35].

The electron trapping energy at a defect level is determined by the long-range Coulomb potential and the short-range potential due to atomic-orbital hybridization [47]. The large static dielectric constants in Bi compounds (see Table II) reduce the long-range Coulomb potential significantly. The low anion coordination numbers of the atomic chain and layered structures of the Bi compounds also reduce the Bi-6p-orbital hybridization at anion vacancies. In the atomic chain structure of Bi chalcohalides as shown in Fig. 2(a), a halogen ion and a chalcogen ion are coordinated to only two and three Bi ions, respectively. It is thus likely that neither the long-range Coulomb potential nor the short-range Bi-6p-orbital hybridization at the anion vacancies is sufficiently strong to create a deep bound state inside the band gap for electron trapping. To test this hypothesis, we studied Se and Br vacancies in BiSeBr using HSE calculations including the SOC.

The ionized Se and Br vacancies have the charge states of $+2$ and $+1$, respectively. The addition of one or two electrons in an anion vacancy causes the Bi atoms near the vacancy to move closer to each other, which is associated with increasing hybridization between the Bi6p orbitals. However, the hybridization is not strong enough to stabilize the trapped electrons due to the small number of Bi neighbors. The defect calculations show that the electron trappings at Se and Br vacancies are both metastable. The calculated $(2+/+)$ transition level for V_{Se} and the $(+/0)$ transition level for V_{Br} are 0.2 and 0.1 eV above the CBM, respectively. Therefore, V_{Se} and V_{Br} are both shallow hydrogenic donor defects, and deep electron trapping by V_{Se} and V_{Br} is not energetically favored. Since the anion vacancies are usually the main native donor defects in halides and chalcohalides, having both V_{Se} and V_{Br} as shallow defects is beneficial to efficient electron transport in BiSeBr.

IV. CONCLUSION

Density functional calculations are carried out to study electronic structure, dielectric properties, optical absorption, and defect properties of selected Bi chalcohalides and oxyhalides (BiSeBr, BiSeI, BiSI, BiOBr) for their potential applications as PV, radiation detection, and transparent conducting materials. BiSeBr, BiSI, and BiSeI have band gaps of 1.3–1.56 eV, suitable for solar energy absorption. The calculated electronic structures suggest the potential applications of *n*-type BiSeBr and *p*-type BiSI and BiSeI in PV technologies. BiSeBr and BiSI may also be used as room-temperature gamma-ray detection materials for their large atomic numbers (for efficient gamma-ray absorption) and large band gaps of >1.5 eV (for room-temperature operation). Since BiSeBr has a small electron effective mass while BiSI has a small hole effective mass, BiSeBr and BiSI detectors should be configured to collect electrons and holes, respectively. BiOBr has a large 3-eV direct band gap and a small hole effective mass, which makes it a potential *p*-type transparent conducting material. Despite having chain structures, BiSI and BiSeI exhibit significant valence-band dispersions in directions both parallel and perpendicular to the atomic chains due to the significant interchain iodine coupling. Similarly, the valence-band dispersion in layered BiOBr is dispersive both on the *ab* plane and along the *c* axis due to the strong interlayer Br-Br coupling. All the Bi compounds shown in this paper have enhanced Born effective charges, leading to strong lattice polarization and anomalously large static dielectric constants. The resulting strong screening of charge defects and impurities should reduce carrier scattering and trapping, which is beneficial to the proposed applications of these materials as PV, radiation detection, and transparent conducting materials. Defect calculations further show that the Se and the Br vacancies in BiSiBr are both shallow donors and thus do not trap electrons effectively, which is important for efficient electron transport. The shallow nature of anion vacancies in BiSeBr is attributed to the strong screening, which suppresses the Coulomb potential, and to the low coordination numbers of anions, which lead to weak hybridization among Bi6*p* orbitals at an anion vacancy.

ACKNOWLEDGMENTS

We are grateful for the helpful discussions with David J. Singh. This work was supported by the Department of Energy, Office of Science, Basic Energy Sciences, Materials Sciences and Engineering Division. This manuscript has been authored by UT-Battelle, LLC under Contract No. DE-AC05-00OR22725 with the U.S. Department of Energy. The United States Government retains and the publisher, by accepting the article for publication, acknowledges that the United States Government retains a non-exclusive, paid-up, irrevocable, worldwide license to publish or reproduce the published form of this manuscript, or allow others to do so, for United States Government purposes. The Department of Energy will provide public access to these results of federally sponsored research in accordance with the DOE Public Access Plan (http://energy.gov/downloads/doe-public-access-plan).

[1] M. A. Green, A. Ho-Baillie, and H. J. Snaith, The emergence of perovskite solar cells, Nat. Photonics **8**, 506 (2014).

[2] https://www.nrel.gov/ncpv/images/efficiency_chart.jpg.

[3] A. V. Churilov, G. Ciampi, H. Kim, L. J. Cirignano, W. M. Higgins, F. Olschner, and K. S. Shah, Thallium bromide nuclear radiation detector development, IEEE Trans. Nucl. Sci. **56**, 1875 (2009).

[4] A. V. Churilov, G. Ciampi, H. Kim, W. M. Higgins, L. J. Cirignano, F. Olschner, V. Biteman, M. Minchello, and K. S. Shah, TlBr and $TlBr_xI_{1-x}$ crystals for Y-ray detectors, Cryst. Growth **312**, 1221 (2010).

[5] S. Johnsen, Z. Liu, J. A. Peters, J. H. Song, S. Nguyen, C. D. Malliakas, H. Jin, A. J. Freeman, B. W. Wessels, and M. G. Kanatzidis, Thallium chalcohalides for x-ray and y-ray detection, J. Am. Chem. Soc. **133**, 10030 (2011).

[6] S. L. Nguyen, C. D. Malliakas, J. A. Peters, Z. Liu, J. Im, L. D. Zhao, M. Sebastian, H. Jin, H. Li, S. Johnsen, B. W. Wessels, A. J. Freeman, and M. G. Kanatzidis, Photoconductivity in Tl_6SI_4: A novel semiconductor for hard radiation detection, Chem. Mater. **25**, 2868 (2013).

[7] M.-H. Du and D. J. Singh, Enhanced Born charge and proximity to ferroelectricity in thallium halides, Phys. Rev. B **81**, 144114 (2010).

[8] M.-H. Du and D. J. Singh, Enhanced Born charges in III-VII, IV-VII_2, and V-VII_3 compounds, Phys. Rev. B **82**, 045203 (2010).

[9] K. Biswas, M.-H. Du, and D. J. Singh, Electronic structure and defect properties of Tl_6SeI_4: Density functional calculations, Phys. Rev. B **86**, 144108 (2012).

[10] M. H. Du, Efficient carrier transport in halide perovskites: Theoretical perspectives, J. Mater. Chem. A **2**, 9091 (2014).

[11] H. Shi and M. H. Du, Native defects in Tl_6SI_4: Density functional calculations, J. Appl. Phys. **117**, 175701 (2015).

[12] P. Ghosez, J.-P. Michenard, and X. Gonze, Dynamical atomic charges: The case of ABO_3 compounds, Phys. Rev. B **58**, 6224 (1998).

[13] R. E. Brandt, V. Stevanović, D. S. Ginley, and T. Buonassisi, Identifying defect-tolerant semiconductors with high mobility-carrier lifetimes: Beyond hybrid lead halide perovskites, MRS Commun. **5**, 265 (2015).

[14] R. E. Brandt, R. C. Kurchin, R. L. Z. Hoye, J. R. Poindexter, M. W. B. Wilson, S. Sulekar, F. Lenahan, P. X. T. Yen, V. Stevanovic, J. C. Nino, M. G. Bawendi, and T. Buonassisi, Investigation of bismuth triiodide (BiI_3) for photovoltaic applications, J. Phys. Chem. Lett. **6**, 4297 (2015).

[15] A. T. Lintereur, W. Qiu, J. C. Nino, and J. E. Baciak, Iodide based compound semiconductors for room temperature gamma-ray spectroscopy, Proc. SPIE **6945**, 694503 (2008).

[16] N. T. Hahn, J. L. Self, and C. B. Mullins, BiSI micro-rod thin films: efficient solar absorber electrodes?, J. Phys. Chem. Lett. **3**, 1571 (2012).

[17] N. T. Hahn, A. J. E. Rettie, S. K. Beal, R. R. Fullon, and C. B. Mullins, n-BiSI thin films: selenium doping and solar cell behavior, J. Phys. Chem. C **116**, 24878 (2012).

[18] X. Zhang, L. Zhang, T. Xie, and D. Wang, Low-temperature synthesis and high visible-light-induced photocatalytic activity of BiOI/TiO2 hetetrostructures, J. Phys. Chem. C **113**, 7371 (2009).

[19] N. T. Hahn, S. Hoang, J. L. Self, and C.B. Mullins, Spray pyrolysis deposition and photoelectrochemical properties of n-type BiOI nanoplatelet thin films, ACS Nano **6**, 7712 (2012).

[20] H. Akkus, Density functional calculation of the electronic structures of some $A^5B^6C^7$-type crystals, Int. J. Mod. Phys. B **23**, 97 (2009).

[21] A. Audzijonis, L. Žigas, G. Gaigalas, R. Sereika, and B. Žygaitiene, Density functional calculation of the photoelectron emission spectra of BiSCl crystal and molecular clusters, J. Cluster Sci. **21**, 577 (2010).

[22] A. Audzijonis, R. Sereika, B. Žygaitiene, and A. Rèza, Optical properties of BiSBr and BiSeBr crystals, J. Phys. Chem. Solids **72**, 1501 (2011).

[23] C. Y. Fong, C. Perlov, and F. Wooten, Electronic properties of BiSeI and BiSeBr, J. Phys. C: Solid State Phys. **15**, 2605 (1982).

[24] Springer Materials, http://materials.springer.com/.

[25] J. P. Perdew, K. Burke, and M. Ernzerhof, Generalized Gradient Approximation Made Simple, Phys. Rev. Lett. **77**, 3865 (1996).

[26] F. Tran and P. Blaha, Accurate Band Gaps of Semiconductors and Insulators with a Semilocal Exchange-Correlation Potential, Phys. Rev. Lett. **102**, 226401 (2009).

[27] D. J. Singh, Structure and optical properties of high light output halide scintillators, Phys. Rev. B **82**, 155145 (2010).

[28] Y.-S. Kim, M. Marsman, G. Kresse, F. Tran, and P. Blaha, Towards efficient band structure and effective mass calculations for III-V direct band-gap semiconductors, Phys. Rev. B **82**, 205212 (2010).

[29] J. Heyd, G. E. Scuseria, and M. Ernzerhof, Hybrid functionals based on a screened Coulomb potential, J. Chem. Phys. **118**, 8207 (2003); Erratum: Hybrid functionals based on a screened Coulomb potential, **124**, 219906 (2006).

[30] A. V. Krukau, O. A. Vydrov, A. F. Izmaylov, and G. E. Scuxeria, Influence of the exchange screening parameter on the performance of screened hybrid functionals, J. Chem. Phys. **125**, 224106 (2006).

[31] J. Paier, M. Marsman, K. Hummer, G. Kresse, I. C. Gerber, and J. G. Angyan, Screened hybrid density functionals applied to solids, J. Chem. Phys. **124**, 154709 (2006).

[32] K. Biswas and M. H. Du, AX centers in II-VI semiconductors: Hybrid functional calculations, Appl. Phys. Lett. **98**, 181913 (2011).

[33] M. H. Du, First-principles study of native defects in TlBr: Carrier trapping, compensation, and polarization phenomenon, J. Appl. Phys. **108**, 053506 (2010).

[34] M.-H. Du and S. B. Zhang, Impurity-bound small polarons in ZnO: Hybrid density functional calculations, Phys. Rev. B **80**, 115217 (2009).

[35] M. H. Du, Density functional calculations of native defects in $CH_3NH_3PbI_3$: Effects of spin-orbit coupling and self-interaction error, J. Phys. Chem. Lett. **6**, 1461 (2015).

[36] P. E. Blöchl, Projector augmented-wave method, Phys. Rev. B **50**, 17953 (1994).

[37] G. Kresse and J. Furthmüller, Efficient iterative schemes for *ab initio* total-energy calculations using a plane-wave basis set, J. Phys. Rev. B **54**, 11169 (1996).

[38] G. Kresse and D. Joubert, From ultrasoft pseudopotentials to the projector augmented-wave method, Phys. Rev. B **59**, 1758 (1999).

[39] P. Blaha, K. Schwarz, G. Madsen, D. Kvasnicka, and J. Luitz, in *WIEN2K: An Augmented Plane Wave+Local Orbitals Program for Calculating Crystal Properties*, edited by K. Schwarz (Technische Universität Wien, Vienna, Austria, 2001), http://www.wien2k.at/.

[40] See Supplemental Material at http://link.aps.org/supplemental/10.1103/PhysRevB.93.104108 for band structures calculated without using the spin-orbit coupling.

[41] Y. Zhou, L. Wang, S. Chen, S. Qin, X. Liu, J. Chen, D.-J. Xue, M. Luo, Y. Cao, Y. Cheng, E. H. Sargent, and J. Tang, Thin-Film Sb_2Se_3 photovoltaics with oriented one-dimensional ribbons and benign grain boundaries, Nat. Photonics **9**, 409 (2015).

[42] S. N. Ahmed, *Physics and Engineering of Radiation Detection* (Elsevier, Amsterdam, 2007).

[43] G. Hautier, A. Miglio, G. Ceder, G. Rignanese, and X. Gonze, Identification and design principles of low hole effective mass p-type transparent conducting oxides, Nat. Commun. **4**, 2292 (2013).

[44] H. Shi, B. Saparov, D. J. Singh, A. S. Sefat, and M. H. Du, Ternary Chalcogenides $Cs_2Zn_3Se_4$ and $Cs_2Zn_3Te_4$: Potential *p*-type transparent conducting materials, Phys. Rev. B **90**, 184104 (2014).

[45] W. J. Yin, T. Shi, and Y. F. Yan, Unusual defect physics in$CH_3NH_3PbI_3$perovskite solar cell absorber, Appl. Phys. Lett. **104**, 063903 (2014).

[46] W. J. Yin, T. Shi, and Y. F. Yan, Unique properties of halide perovskites as possible origins of the superior solar cell performance, Adv. Mater. **26**, 4653 (2014).

[47] H. Shi and M. H. Du, Shallow halogen vacancies in halide optoelectronic materials, Phys. Rev. B **90**, 174103 (2014).